Assessment of Arctic sea ice freeboard from photon-counting laser altimetry: Pre-launch activities for NASA's ICESat-2 Mission

Julia M. Ruth[1], Sinead L. Farrell[2,3], Kelly M. Brunt[3]

[1]Physics Department, University of Maryland [2]Earth System Science Interdisciplinary Center, University of Maryland [3]Goddard Earth Sciences Technology And Research Program, Morgan State University

Introduction

Sea ice mass balance and thickness are leading indicators of the state of the global climate system. Understanding the nature and variability of Arctic and Southern Ocean sea ice, and its contribution to the global climate system, is critical. NASA currently operates a number of airborne missions designed to measure Arctic sea ice thickness. Experiments are designed to better understand conventional and emerging laser altimetry techniques in achieving this goal.

April 2012 – Sea Ice Survey

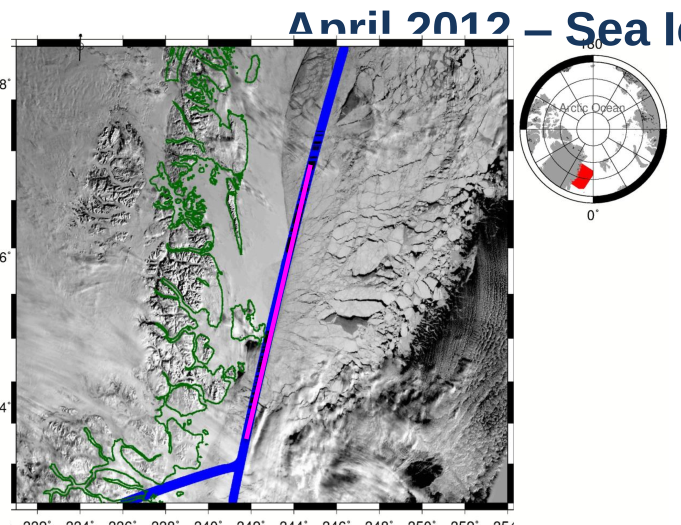

Figure 1: Map of survey lines over sea ice in the Greenland Sea conducted on 10 April 2012 by two NASA aircrafts.

An airborne survey took place over Arctic sea ice on April 10, 2012, in which the NASA P-3B carrying the Operation IceBridge (OIB) instrument suite (*Koenig et al.*, 2011) surveyed the sea ice in the Fram Strait and the western Greenland Sea. Concurrently, a second NASA aircraft, the ER-2, carrying the Multiple Altimeter Beam Experimental Lidar (MABEL), flew in tandem along the same flight line [**Figure 1**].

This study focuses on an assessment of MABEL via comparison with data from two OIB instruments: the Airborne Topographic Mapper (ATM) and the Digital Mapping System (DMS) Camera. We also make use of MODIS satellite imagery over the survey site.

Experiment Goals – Preparing for ICESat-2

By comparing the spatially-coincident data from the two NASA flight surveys, we assess MABEL photon-counting altimetry over Arctic sea ice. MABEL is an airborne simulator for the Advanced Topographic Laser Altimeter System (ATLAS), the primary instrument to be flown on ICESat-2. The goal of the MABEL experiments is to test the instrument theory for ICESat-2 (*Brunt et al.*, 2013). ICESat-2 is the second NASA Earth-observation mission dedicated to monitoring the polar regions, following the successful ICESat mission which operated between 2003 and 2009. A key mission goal for ICESat-2 is to accurately measure basin-scale sea ice thickness (*Abdalati et al.*, 2010). ICESat-2 will have a multibeam, photon-counting laser altimeter operating at 532 nm, with high-resolution 10 m footprints, separated at 0.7 m along-track [**Figure 2**].

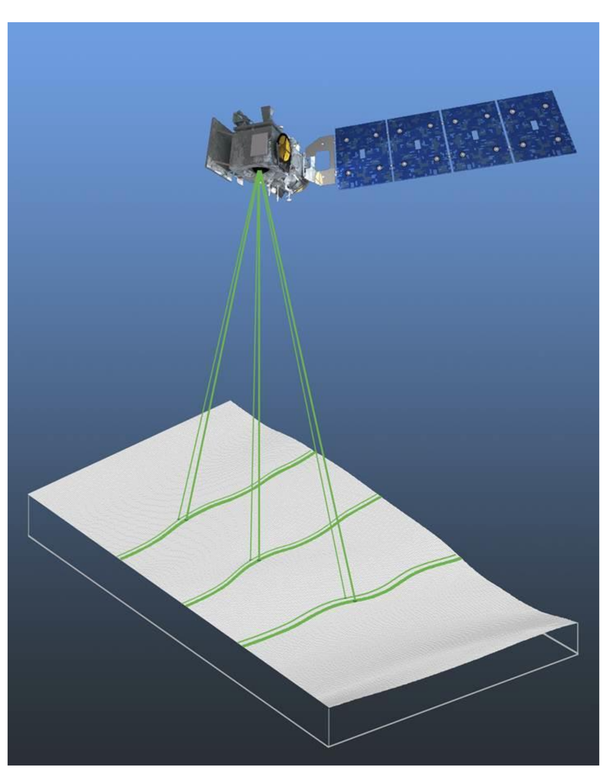

Figure 2: Artist's impression of NASA ICESat-2 laser altimetry mission, due for launch in 2016.

Accounting for Ice Drift

Since the NASA aircraft operate at different flight speeds, resulting in a shift in temporal sampling between the two surveys, we correct for the effects of sea ice drift. Drift rates were determined by comparing the geolocations of specific sea ice features (e.g. pressure ridges) in the north-bound ATM data set with the south-bound ATM data set [**Figure 3a**]. Velocity vectors were mapped over MODIS satellite imagery to help correct for the temporal offset between the OIB airborne data and the ER-2 MABEL data [**Figure 3b**]. This method yielded an average drift rate of 24.61 cm/s. Our calculated drift rates agreed with an independent estimate of sea ice drift, derived from a combined Advanced SCATterometer (ASCAT) and Special Sensor Microwave/Imager (SSMI) product available at: CERSAT/Ifremer (http://cersat.ifremer.fr/).

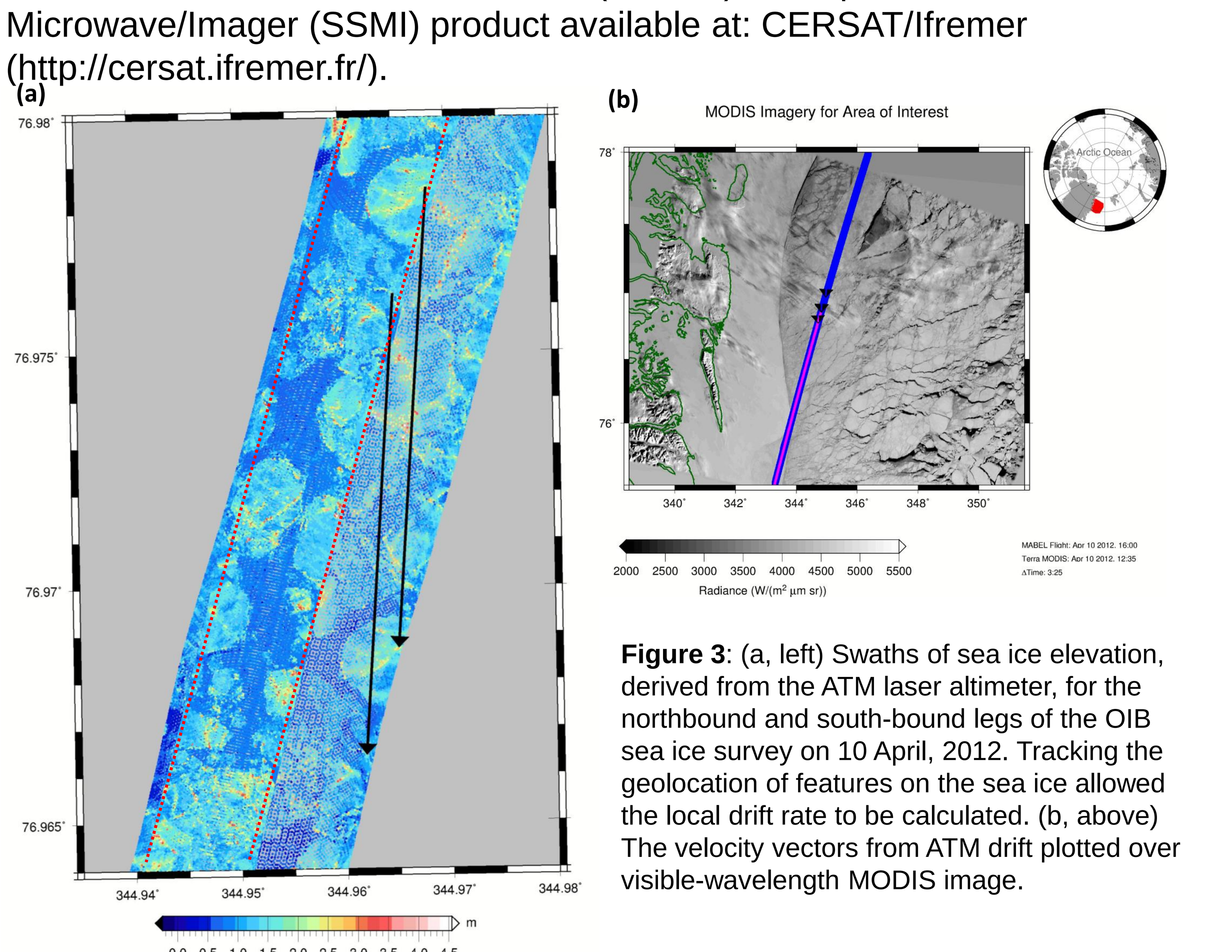

Figure 3: (a, left) Swaths of sea ice elevation, derived from the ATM laser altimeter, for the northbound and south-bound legs of the OIB sea ice survey on 10 April, 2012. Tracking the geolocation of features on the sea ice allowed the local drift rate to be calculated. (b, above) The velocity vectors from ATM drift plotted over visible-wavelength MODIS image.

References:

Abdalati, W., H. J. Zwally, R. Bindschadler, B. Csatho, S. L. Farrell, H. A. Fricker, D. Harding, R. Kwok, M. Lefsky, T. Markus, A. Marshak, T. Neumann, S. Palm, B. Schutz, B. Smith, J. Spinhirne, C. Webb (2010), The ICESat-2 Laser Altimetry Mission, *Proc. IEEE*, *98*(5), 735 – 751, doi: 10.1109/JPROC.2009.2034765

Brunt, K.M., T.A. Neumann, K.M. Walsh, and T. Markus (2013), Determination of local slope on the Greenland Ice Sheet using a multibeam photon-counting lidar in preparation for the ICESat-2 mission, *IEEE Geosci. Rem. Sens. Lett., 11(3)*, doi:10.1109/LGRS.2013.2282217, *in press*.

Koenig, L., S. Martin, M. Studinger, and J. Sonntag (2010), Polar Airborne Observations Fill Gap in Satellite Data, *EOS Trans. AGU,* 91(38), 333-334.

Kwok, R., S. L. Farrell, T. Markus and J. Morrison (2013), ICESat-2 Algorithm Theoretical Basis Document (ATBD) forSea Ice Products, NASA Technical Memorandum, *draft.*

Photon-Counting Lidar Altimetry

The first experiments over polar ice occurred in April 2012, when MABEL collected altimetric measurements over both land and sea ice. MABEL is a photon-counting, multibeam lidar operating at two wavelengths: 532 and 1064 nm. Assuming a nominal flight altitude, the MABEL footprints are ~ 2 m, spaced ~ 4 cm along-track (*Brunt et al.*, 2013). Here we make use of data collected in the visible spectrum (532 nm): channels 5 and 6, when MABEL operated at 5kHz.

Figure 4 illustrates a 28-km segment of MABEL data gathered in the Greenland Sea, showing elevation measurements over both rough sea ice and smoother leads. Raw, unfiltered data are shown (top) which include signal photons reflected from the sea ice/ocean surface, and background noise photons, due to solar contamination. The first step applies the Goddard Space Flight Facility (GSFC) Surface-Finding algorithm, a histogram-based approach outlined in *Brunt et al.* (2013), to distinguish signal from noise photons, leaving only data points associated with the surface return (middle). Second, we apply an along-track median filter, operating at 50 m, to further reduce noise and extract the surface response of the lidar (bottom). Using data from the leads only, we calculated the precision of the MABEL data. Our results are outlined in **Table 1**.

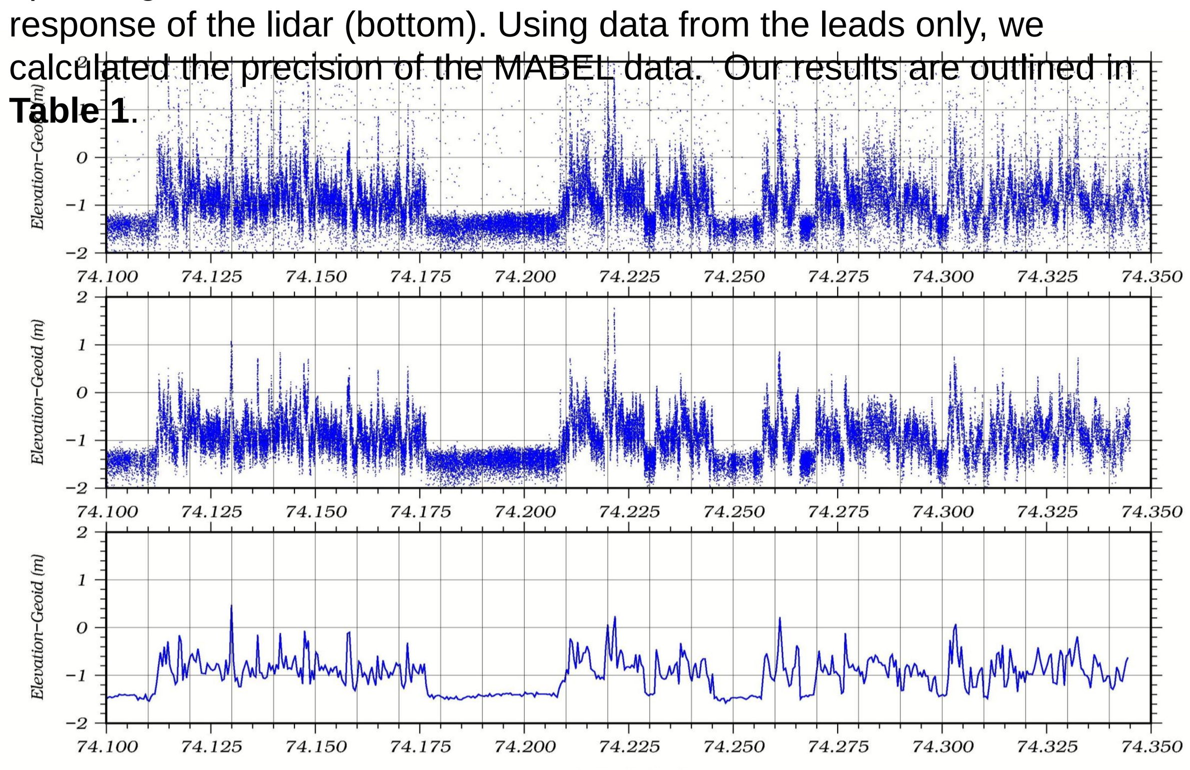

Figure 4: MABEL data profiles for Channel 5 demonstrating the noise in the raw data (top), the extraction of the signal photons –after application of the GSFC Surface Finding Algorithm (middle), and the final dataset (bottom) after application of a 50-point along-track median filter.

Data set	Standard Deviation (m)	Data Points (#)
Raw MABEL (signal + noise photons)	16.85	17116
GSFC Surface Finding Algorithm	0.15	11052
Filtered MABEL (50 point median filter)	0.042	119

Table 1. To estimate of MABEL measurement precision we calculate the standard deviation of elevations over 5 leads. We find the precision of the filtered MABEL data is 0.042 m.

Processing MABEL Data over Sea Ice

In order to compare the MABEL profiles to the ATM and DMS data, ice drift between the two flight times had to be accounted for. Using a drift rate of 24.61 cm/s, and the time elapsed between MABEL and ATM acquisitions, we adjusted the geolocation of the MABEL data. An additional delta was applied, based on ridges that were apparent in both data sets, to fine-tune the drift correction and account for the increased drift experienced in the southern portion of the flight survey. We also applied an absolute elevation bias correction to the MABEL data, following *Brunt et al.* (2013) to account for offsets in the channel mountings. The bias corrections were -1.9855 m and -1.7555 m for channels 5 and 6, respectively.

Coincident DMS visible imagery were assessed to extract pixel brightness at each point along the lidar beam paths. An example of this is shown in **Figure 5**. A pixel brightness threshold of less than 40 was assigned to discriminate the presence of leads (Figure 5, bottom panels). This value was chosen to include open water and very thin ice, while excluding refrozen leads with snow accumulation. Using this threshold, elevation measurements associated with leads were distinguished (e.g. cyan and light-pink points, Figure 5, top panels). The mean of the lead elevation distribution was assigned as the local sea surface height (SSH) and a one-sigma edit was performed to further refine this mean value and discard anomalous values. This approach was applied to MABEL channel 5 and 6 data, and to the ATM elevation measurements, to extract lead elevations and obtain a SSH profile for each set of lidar data. The method was applied to short along-track segments ~ 28 km in length.

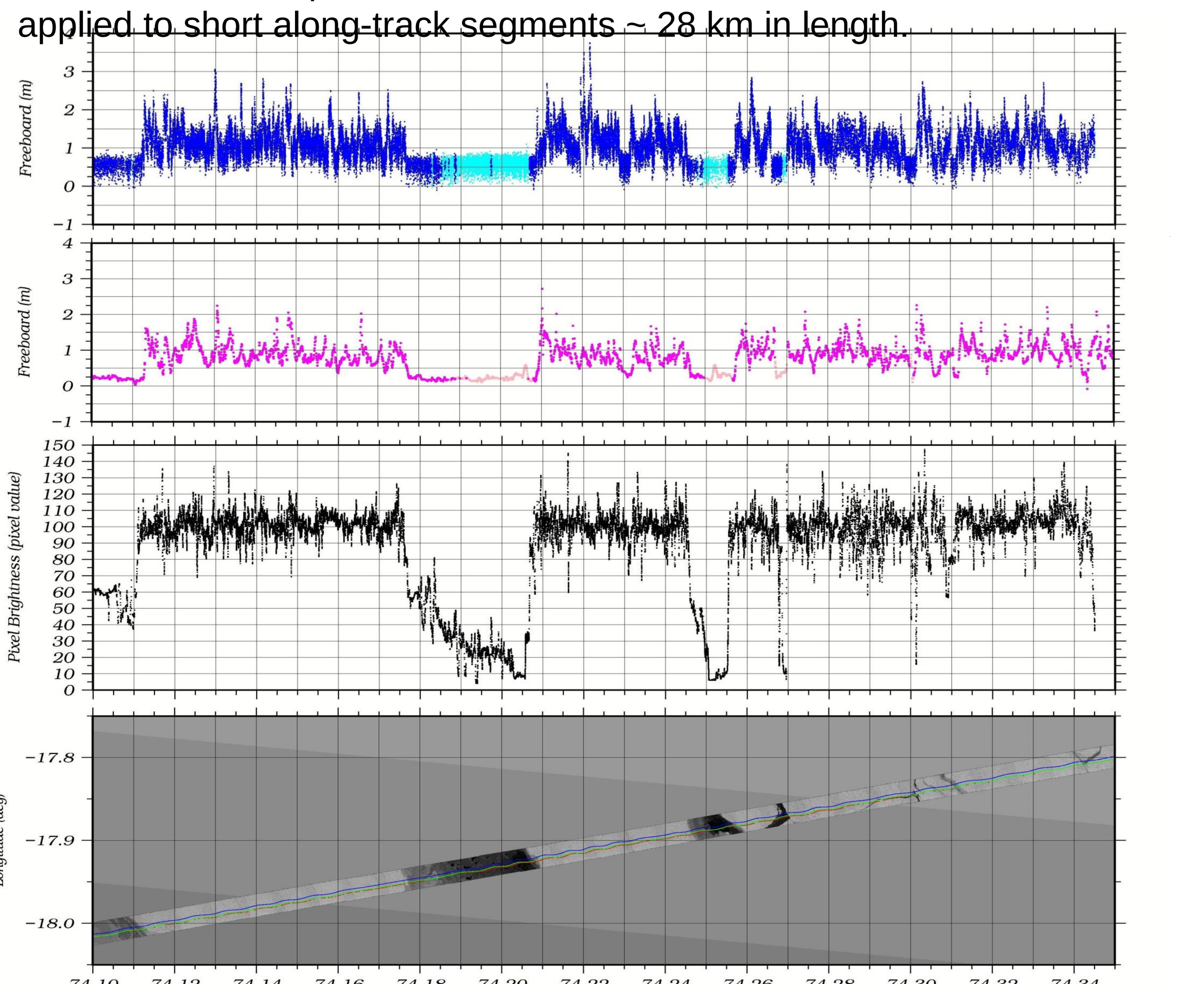

Figure 5: Analysis of a 28-km long section of MABEL, ATM, and DMS data along the flight line demonstrates the process of distinguishing lead elevations within the along-track profiles. This method is used to define the local sea surface height for extraction of ice freeboard.

Results

Once the local SSH profiles were established, the SSH was subtracted from each elevation measurement to derive along-track freeboard for both the MABEL and ATM data sets. We derived sea ice freeboard estimates at four case-study locations along the survey line. These 28-km long segments were associated with a range of sea ice conditions. **Figure 6a** shows the resulting freeboard distributions obtained for Case Studies 1, 3 and 4, and compares the freeboard derived from MABEL channel 5 (blue), channel 6 (green) and from the ATM (magenta). Overall there was good agreement between the freeboard derived from the ATM laser, compared to MABEL, although the modal MABEL freeboard was typically lower than the modal ATM freeboard, by 10 – 20 cm. This may be a result of the along-track median filtering applied to the MABEL data and further work is required to understand the impacts of this filtering.

Case study 2 did not contain any leads except for sparse fractures and thus freeboard could not be determined. **Figure 6b** demonstrates the sea ice elevation distribution in Case Study 2, for the MABEL data after application of the GSFC Surface Finding Algorithm (solid blue), the MABEL data after of the median filter (dashed blue), and the ATM data (magenta).

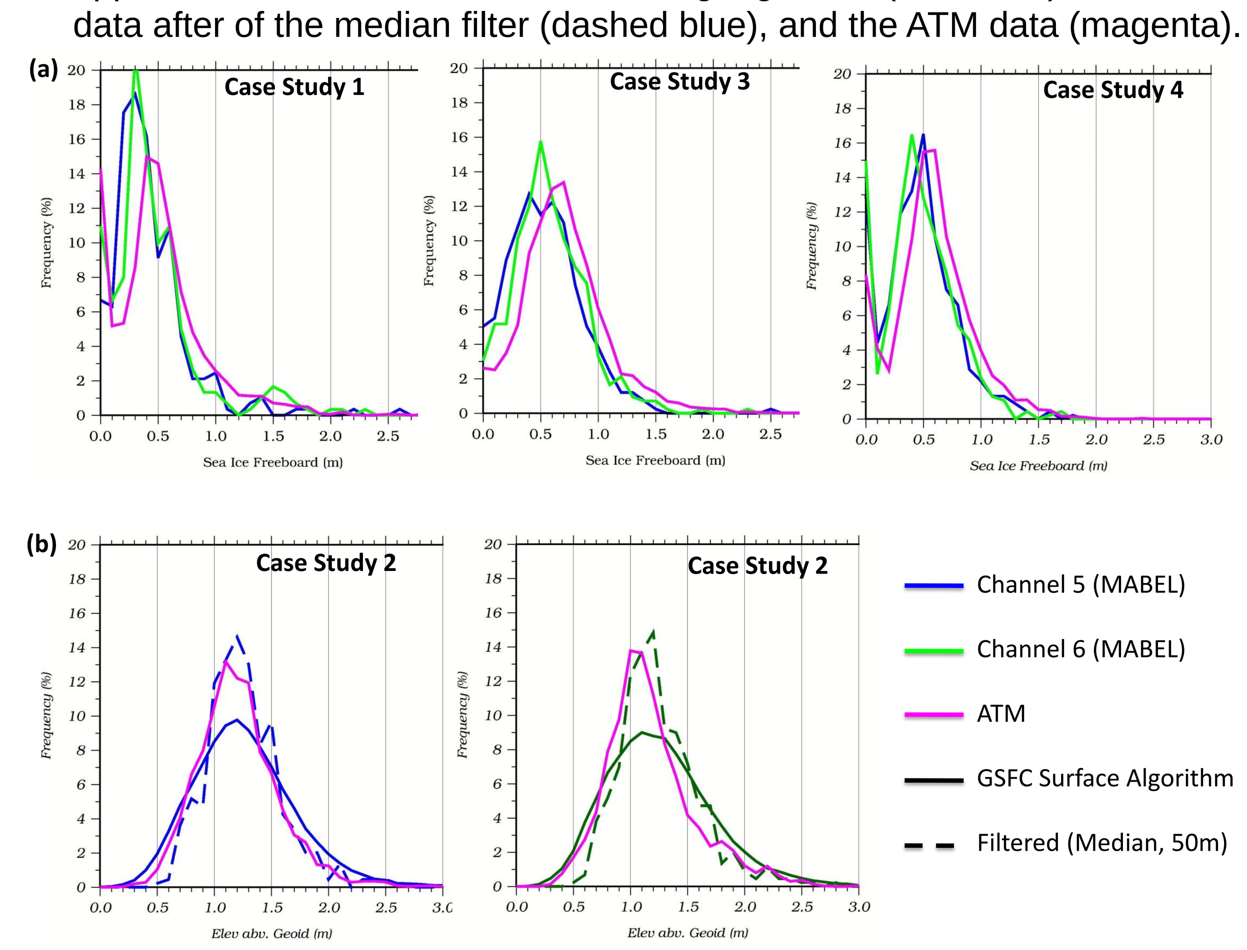

Figure 6a (top row): Sea ice freeboard distributions in the three case study areas where leads were prevalent enough to allow SSH to be determined.
Figure 6b (bottom row): Sea ice elevation distributions in a region of sea ice with frequent ridges.

Case Study 1	**Data Set**	**Mean**	**Mode**	**Data Points (#)**
	Freeboard Channel 5	0.382	0.357	340
	Freeboard Channel 6	0.438	0.389	341
	ATM	0.511	0.487	44000
Case Study 3	**Data Set**	**Mean**	**Mode**	**Data Points (#)**
	Freeboard Channel 5	0.541	0.530	444
	Freeboard Channel 6	0.595	0.575	445
	ATM	0.715	0.703	64612
Case Study 4	**Data Set**	**Mean**	**Mode**	**Data Points (#)**
	Freeboard Channel 5	0.409	0.427	557
	Freeboard Channel 6	0.410	0.417	557
	ATM	0.567	0.582	72240
Case Study 2	**Data Set**	**Mean**	**Mode**	**Data Points (#)**
	Elevation Channel 5 (GSFC Surface)	1.313	1.275	77518
	Elevation Channel 6 (GSFC Surface)	1.309	1.265	88140
	Elevation Channel 5 (Filtered)	1.314	1.265	446
	Elevation Channel 6 (Filtered)	1.301	1.247	445
	ATM under Channel 5	1.260	1.231	77518
	ATM under Channel 6	1.228	1.163	88140

Table 2: Sea ice freeboard results (mean, modal freeboard, m) are shown for case studies 1,3 and 4. Freeboard derived from two MABEL channels (5 and 6) are compared to freeboard estimates from the ATM lidar system. Sea ice elevations are shown for case study 2 since no leads were present.

Conclusions and Further Work

The results show that the freeboard distributions derived from the two independent airborne lidar sensors (MABEL and ATM) were consistent for all case studies. The ATM elevation measurements were however consistently higher than those from MABEL for Case Studies 1, 3, and 4, where freeboard was evaluated. Further work is required to understand this difference and the impact of the along-track median filtering, as well as noise on the ATM measurements.

In the region where no leads were present (case study 2), we have demonstrated that the application of along-track median filtering to the MABEL data produces more consistent results when compared to the ATM elevations.

We have demonstrated that the MABEL sensor is effective for determining sea ice freeboard in this region.

Future work will be to process the additional MABEL data gathered over sea ice during the April 2012 mission. Following initial work by *Kwok et al*. (2013) to define an automated sea ice freeboard algorithm for use on-board ICESat-2, we will investigate an automated approach for deriving "quick-look" sea ice freeboard estimates from MABEL data. This algorithm is specifically designed to operate in the Marginal Ice Zone, and is used as a feasibility test for producing near-real-time (or "quick look") sea ice freeboard estimates from ICESat-2.

Acknowledgements: I wish to thank the following collaborators for their assistance with this research project, including:

Sinead Farrell (ESSIC): Outstanding project mentor and general project assistance
Kelly Brunt (NASA GSFC): Project collaborator and assistance with processing MABEL photon-counting data
Nathan Kurtz, Vincent Onana, Jeremy Harbeck (NASA GSFC) and Tom Newman (ESSIC): Assistance with processing DMS imagery
Larry Connor (NOAA LSA): Assistance with processing ATM laser data

We thank the NASA Operation IceBridge and ICESat-2 Projects for their dissemination of the ATM, DMS and MABEL data sets.

ICESat-2 ICE, CLOUD, AND LAND ELEVATION SATELLITE-2

Laboratory for Satellite Altimetry NOAA-NESDIS-STAR